RAA 2020 Vol. **20** No. **8**, 133(9pp) doi: 10.1088/1674–4527/20/8/133

http://www.raa-journal.org *http://iopscience.iop.org/raa*

***R**esearch in*
***A**stronomy and*
***A**strophysics*

Eclipsing binary XZ CMi in a hierarchical quadruple system

Zhi-Hua Wang and Li-Ying Zhu

Yunnan Observatories, Chinese Academy of Sciences, Kunming 650216, China; *wzh@ynao.ac.cn*
Key Laboratory for the Structure and Evolution of Celestial Objects, Chinese Academy of Sciences, Kunming 650216, China
Center for Astronomical Mega-Science, Chinese Academy of Sciences, Beijing 100101, China
University of Chinese Academy of Sciences, Beijing 100049, China

Received 2020 February 20; accepted 2020 April 2

Abstract The new complete BVR_cI_c light curves and spectra of the short-period eclipsing binary XZ CMi are presented. The results from the combined analysis based on the photometric and spectroscopic data show that XZ CMi is a near contact binary with the secondary component filling its critical Roche lobe while the primary filling 91% of its Roche lobe. The investigation of the $O-C$ diagram reveals that its orbital period is continuously increasing, which is consistent with the derived configuration and caused by the mass transfer from the less massive star to the more massive one. In addition, an obvious periodic modulation with the amplitude of0.0187(±0.0016) d and a high eccentric of 0.86(±0.04) is detected, which could be the results of the light time effect as a third star with the mass no less than 0.42(±0.09) $M_\odot$ orbiting around the central eclipsing binary once every 95.7(±2.1) yr. Furthermore, we found a visual companion star at $2.4''$ east by south of this system at a much greater distance by direct image. The large third light contribution found from the light curve analysis could be well explained by the existence of the third star and the fourth visual one. The similar parallax and proper motion imply that the components of this hierarchical quadruple system might be bounded by gravitation. Spectroscopic observations for two visual components were carried out by the LAMOST and 2.16 m telescopes, respectively. Their different values of [Fe/H] suggest that they were not born from the same origin. Thus, XZ CMi system is an interesting and important target to study the formation of the multiple stars.

Key words: binaries: close — binaries: eclipsing — stars: individual (XZ CMi)

1 INTRODUCTION

Near contact binaries are a subclass of close binary that contains two close-in companion stars. Both of the components have almost filled their inner critical Roche lobes. The primary star of an Algol-type near contact binary should commonly have a high filling degree. They also usually present the EA or EB type light curves. This typical kind of close binary lays in a key evolutionary status.

Visual wide binaries are in a weakly gravitational bound alliance. Jiménez-Esteban et al. (2019) recently published the *Gaia* DR2 catalogue for comoving wide binary population, where they consider $\sim$ 400 to 500 000 au as the candidates. In the sight of Motte et al. (1998), the size of a primordial wide binary is restricted for the modest core of a star forming region, typically less than 10 000 au. Kouwenhoven et al. (2010) brought the idea that wide binaries might be formed during the star cluster dissolution phase. Stars could also be captured by another from the relatively dense interstellar field. Wide binaries provides a great probe to investigate the evolution and dynamics of close binary/multiple systems and even of star clusters. In particular for the binary + single systems, the farther star might play a relatively significant role in driving central binary merge (Hamers & Samsing 2019).

Eclipsing binary XZ CMi (α_{2000} = 07:54:07.07, δ_{2000} = +03:39:20.34) was first declared as an Algol-type system by Hoffmeister (1934). Soon afterwards in 1938, Lause (1938) published the first light curve showing that it belongs to an EA type. Since then a growing number of researchers have been firmly committed to the photometric observation of this target. Many of them have reported the times of light minimum, such as, Dueball & Lehmann (1965), Gimenez & Costa (1979), Terrell et al. (1994), Zejda et al. (2006), Samolyk (2009), Hubscher (2015), etc.

Secular and cyclic orbital period changes were analyzed by Qian (2002), Samec et al. (2006), and Kim et al. (2009). Investigations of photometric solutions for XZ CMi based on observational light curves continued for decades, although they have not come to an agreement. For example, the effective surface temperature of the primary companion differs from 7000 K to 8876 K, and the derived mass ratio ranges from 0.293 to 0.83 (Mardirossian & Giuricin 1981; Rafert 1990; Terrell et al. 1994; Terrell & Henden 2002; Samec et al. 2006; and Kim et al. 2009). By surveying the database of the *Gaia* satellite, it is found that the effective temperature of XZ CMi is 7079 K and the mean apparent magnitude in the *Gaia*-g band is 10.15 mag with the distance of about 314($\pm$4) pc away (Gaia Collaboration et al. 2018). As is stated in the paper of Terrell & Henden (2002), Henden took an image of a dim object at an angular distance of 2.452 (error within 0.1) arcsec east by south of XZ CMi with an I_c filter. It seems to be a visual companion star (here after the ViS) .

This study sets out to investigate the light curve modelling, timing variation and visual companion of this system. Photometric and spectroscopic observations are discussed in Section 2. The orbital period change is analysed in Section 3 with all the times of eclipse minima. An updated photometric solution by using the input parameters obtained with the spectroscopic method is performed in Section 4. In the last section, we discuss on the orbital period evolution, the visual system and the photometric solutions.

2 OBSERVATIONS

2.1 Photometric Observations

Our first photometric survey for XZ CMi can be dated back to 2008. While the follow-up observation lasted to 2019. In total, 18 new times of light minimum were obtained and listed in Table 1. They were observed on 2008 Feb 1, 2018 Mar 29, 2018 Apr 9, 2019 Jan 25 and 2019 Feb 4 with the 1 m and 60 cm Cassegrain reflecting telescopes located at Yunnan Observatories CAS. During the observations the exposure time for these observations with 60 cm telescope are 80s, 40s, 30s and 20s in BVR_CI_C bands, with 1 m telescope are 30s, 20s and 10s in VR_CI_C bands, and with 80 cm telescope are 25s, 20s, 15s and 10s in BVR_CI_C bands. Data processes were carried out by using the IRAF (Image Reduction and Analysis Facility) software and the method of differential photometry.

The BVR_CI_C four color light curves of XZ CMi within a total phase were observed by using the Tsinghua-NAOC 80 cm telescope on 2018 Nov 9, 2018 Nov 11, 2018 Nov 12 and 2019 Jan 25. This classic Cassegrain reflecting telescope equipped with the VersArray 1300B CCD photometric detector and with the field of view of about $11.5^{'} \times 11.2^{'}$ is placed at the Xinglong Observatory, NAOC, CAS (Huang et al. 2012). During the observations in the four clear nights, the corresponding exposure time of the standard Johnson-Cousins' B, V, R_C and I_C filters were set as 25s, 20s, 15s and 10s, respectively. Data process were also carried out by using the IRAF software and the method of differential photometry. The period 0.578809 d was used to calculate the phase, and the photometric four color light curves of XZ CMi are shown in Figure 1.

2.2 Spectroscopic Observations

The Large Sky Area Multi-Object Fiber Spectroscopic Telescope (LAMOST) is a special quasi-meridian reflecting Schmidt telescope located at the Xinglong Observatory. LAMOST has 4000 fibers for the targets input simultaneously, promising a very high spectrum acquiring rate (Cui 2009; Zhao et al. 2012). Many close binaries and variable stars were observed and investigated by LAMOST (e.g., Qian et al. 2017; Qian et al. 2018; Qian et al. 2019a; Qian et al. 2019b; Zhang et al. 2019). On the day Nov 9 2014, one of the input targets was originally intended to be XZ CMi ($\alpha_{2000} = 118.529448°$, $\delta_{2000} = +03.655646°$), whereas, coincidentally pointed to the ViS ($\alpha_{2000} = 118.530084°$, $\delta_{2000} = +03.655476°$). It means that the spectroscopic observation by LAMOST is actually belongs to the ViS rather than XZ CMi.

To investigate the spectroscopic property of the binary pair XZ CMi, we conducted observations with the 2.16 m telescope at Xinglong station at two clear nights, 2019 May 1 and 2019 May 2. During these observations a $G7$+$S1$-8+$385LP$ grating was used. The spectroscopic diagram shown in Figure 3 and the spectroscopic parameters tabulated in Table 2 are obtained by using the ULySS (University of Lyon Spectroscopic analysis Software).

We took an image of XZ CMi in the VR_cI_c bands at a 'good-seeing' night with the 2.16 m telescope at Xinglong station on 2019 May 1. As shown in Figure 2, there is a nearby dim 'Visual Star' at the east by south of XZ CMi that gradually brightened along with the wavebands.

3 THE $O-C$ ANALYSIS

$O-C$ curve of XZ CMi was analysed by Qian (2002), Samec et al. (2006), Kim et al. (2009), although it does not trace the trend by adding the newly observed data (Fig. 4). To get a better description of the $O-C$ curve, we reanalysed it. Together with our new observations and those from literature, a total of 90 DASCH (Digital Access to a Sky Century at Harvard) data, 78 visual and photographic data, and 120 photoelectric and CCD data were compiled

Table 1 New Light Minima for XZ CMi

HJD	Error	Filter	Telescope	Obs-date
2454498.10175	0.00013	V	1 m (YNOs)	2008-02-01
2454498.10153	0.00014	R_C	1 m (YNOs)	2008-02-01
2454498.10130	0.00010	I_C	1 m (YNOs)	2008-02-01
2458207.12485	0.00021	B	60 cm (YNOs)	2018-03-29
2458207.12487	0.00021	V	60 cm (YNOs)	2018-03-29
2458207.12480	0.00015	R_C	60 cm (YNOs)	2018-03-29
2458207.12454	0.00015	I_C	60 cm (YNOs)	2018-03-29
2458218.12361	0.00023	B	60 cm (YNOs)	2018-04-09
2458218.12345	0.00036	V	60 cm (YNOs)	2018-04-09
2458218.12336	0.00034	R_C	60 cm (YNOs)	2018-04-09
2458218.12343	0.00023	I_C	60 cm (YNOs)	2018-04-09
2458519.10457	0.00016	V	60 cm (YNOs)	2019-02-04
2458519.10430	0.00019	R_C	60 cm (YNOs)	2019-02-04
2458519.10447	0.00025	I_C	60 cm (YNOs)	2019-02-04
2458509.26425	0.00012	B	80 cm (Tsinghua-NAOC)	2019-01-25
2458509.26407	0.00007	V	80 cm (Tsinghua-NAOC)	2019-01-25
2458509.26406	0.00024	R_C	80 cm (Tsinghua-NAOC)	2019-01-25
2458509.26346	0.00014	I_C	80 cm (Tsinghua-NAOC)	2019-01-25

Table 2 Spectral Parameters of XZ CMi and the ViS

Target	T (K)	$\log g$ (m s^{-2})	[Fe/H] (dex)	Telescope	Date
XZ CMi	6920($\pm$73)	4.11($\pm$0.20)	–0.141($\pm$0.005)	2.16 m	2019-05-01
XZ CMi	7016($\pm$99)	4.13($\pm$0.23)	–0.125($\pm$0.017)	2.16 m	2019-05-02
the ViS	6164($\pm$18)	4.61($\pm$0.03)	0.108($\pm$0.016)	LAMOST	2014-11-09

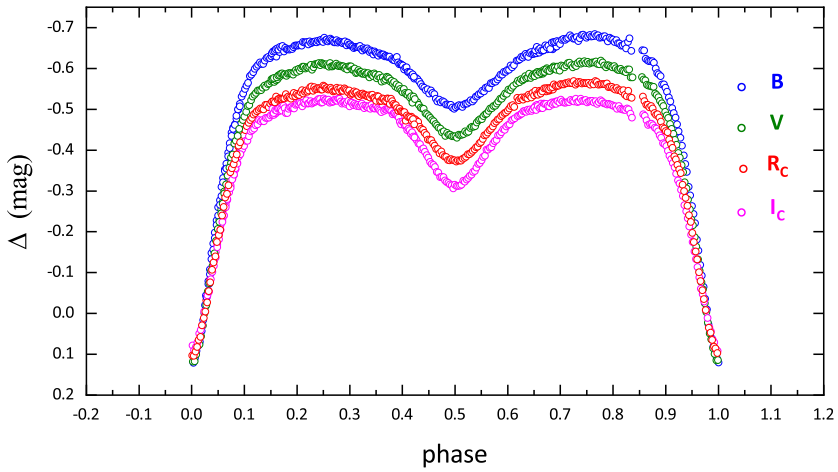

Fig. 1 CCD Photometric LCs of BVR_cI_c bands observed with the 80 cm telescope.

for fitting with the weight of 0.1:1:6. By using the linear ephemeris $\mathrm{Min.I} = \mathrm{HJD}\ 2445404.4387 + 0.^{\mathrm{d}}578809 \times E$, the epoches ($E$) and the corresponding $O-C$ were calculated.

By considering the combination of a quadratic term overlying an extra term (τ), and nonlinear least square and the Levenberg-Marquardt algorithm, the formula could be written as follows,

$$O - C = \Delta T_0 + \Delta P_0 \times E + \frac{1}{2} P^{'}(0) \times E^2 + \tau. \quad (1)$$

τ is to describe the eccentric orbit (Irwin 1952), $\tau = K\left[\sqrt{(1-e_3^2)}\sin E_a \cos\omega + \cos E_a \sin\omega\right]$, where the oscillating amplitude is $K = a_{12}\sin i^* \sqrt{(1-e_3^2\cos^2\omega)}/c$, c is the speed of light in vacuum, a_{12} is the semi-major axis of the orbit that the eclipsing binary is orbiting, e_3 is the eccentricity of the third-body, i^* is the inclination, ω is the longitude of the periastron, and E_a is the eccentric anomaly.

The fitting curves are plotted in Figure 5. As can be seen from the figure, the smallest dots refer to the DASCH data, the bigger dots to the other visual and photographic data, and the biggest dots to the photoelectric and CCD data. Both the long-term change and the short-term variation are continuous and well fitted by the lines. The middle pan-

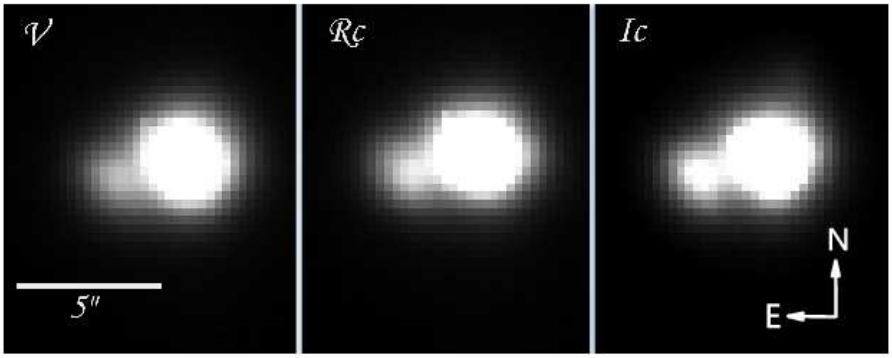

Fig. 2 The VR_cI_c band direct image of the visual binary with the Xinglong 2.16 m telescope on 2019 May 1.

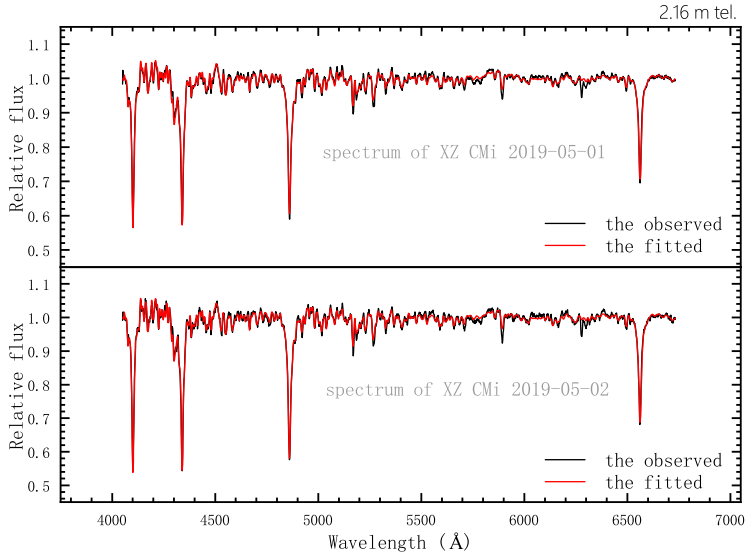

Fig. 3 Normalized spectrum of eclipsing binary XZ CMi with the Xinglong 2.16 m telescope on 2019 May 1 and 2019 May 2.

el of Figure 5 shows the periodic oscillation, of which the open-up parabola had been deducted from the combined fitting line in the upper panel. The parameters are listed in Table 3 where the amplitude of the periodic variation is 0.0187(±0.0016)d, and the period is so long as to be about 95.7(±2.1)yr. No other changes could be extracted from the final residuals presented on the bottom.

4 MODELLING THE LIGHT CURVES

Light-curves in BVR_CI_C bands were observed and modelled with the 2013 version WD programme (Wilson & Devinney 1971; Wilson 1979). The first spectroscopic observations for XZ CMi were also carried out on 2019 May 1 and 2. The mean effective temperature is measured to be 6968(±87) K, and then we also took 6881 K and 7055 K as input values of T_1. The gravitational-darkening coefficients was set as $g_1 = g_2 = 0.32$ (Lucy 1967), and the bolometric albedo to be $A_1 =$

Table 3 Parameters of Period Change and Light-time Effect

Parameter	Value
$\triangle T_0$	–0.01122(±0.00051)
$\triangle P_0$	9.42(±0.33) $\times 10^{-7}$
$P^{'}(0)$ (d cyc^{-1})	1.29(±0.34) $\times 10^{-11}$
K (d)	0.0187(±0.0016)
e	0.86(±0.04)
ω (°)	–141.8(±4.5)
P_3 (yr)	95.7(±2.1)
$f(m)$ ($M_\odot$)	0.0092(±0.0057)
$m_{3\min}$ ($M_\odot$)	0.42(±0.09)
$a_{3\max}$ (au)	25.2(±5.7)

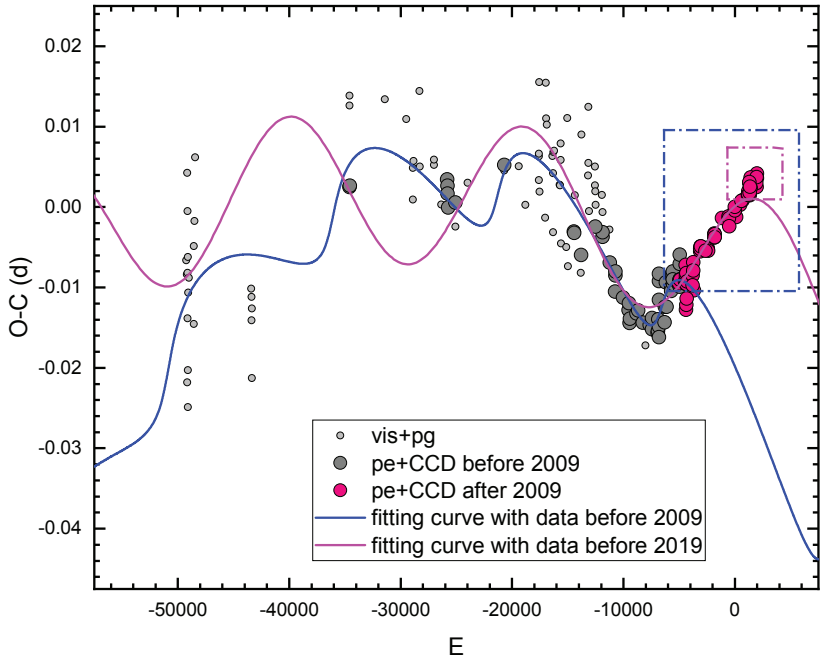

Fig. 4 The former analysis of $O-C$ curve before 2009.

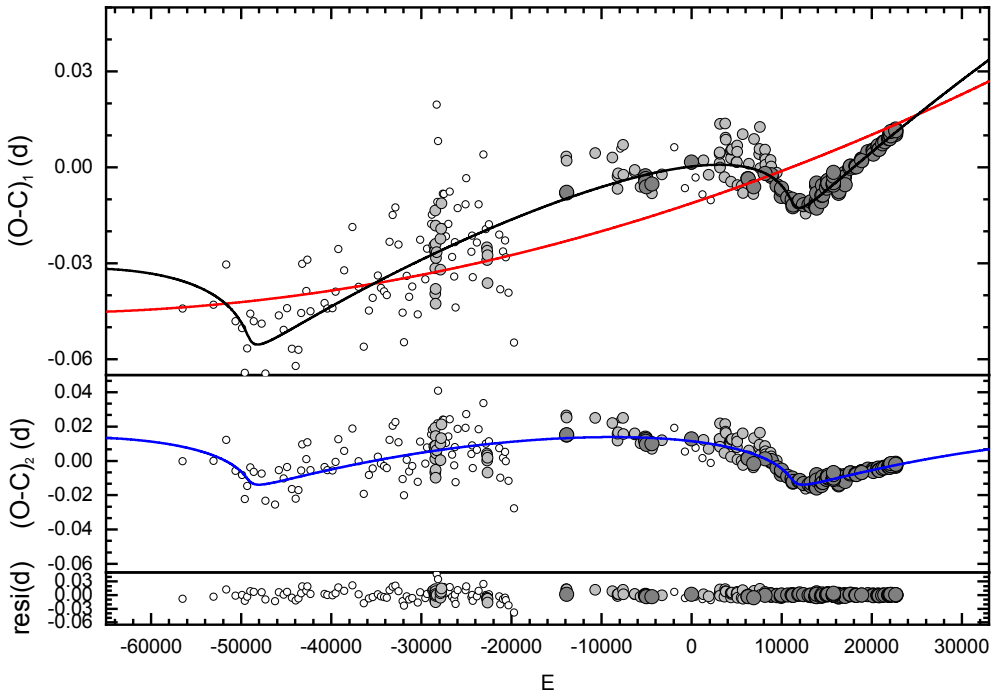

Fig. 5 Our $O-C$ curve where the *smallest dots* are data from DASCH, the *middle dots* are visual and photographic data, and the *biggest dots* are photoelectric and CCD data.

$A_2 = 0.5$ (Ruciński 1969). In addition, the bolometric and bandpass limb-darkening coefficients are acquired according to van Hamme (1993). Meanwhile, parameters such as the inclination i, temperature T_2, primary monochromatic luminosity l_{1B}, l_{1V}, l_{1Rc} and l_{1Ic}, and the dimensionless surface potentials Ω_1 and Ω_2 are all self-adaption with the iteration of the program.

Different models of the WD code were tried, and only mode 5 (semi-detached binary with the secondary filling its equipotential surface) is considered as the appropriate model. As has been shown on the left of Figure 6, a series of q were tried, generating the optimal convergence solution. The parameters are tabulated in Table 4, where one can see the value of q is 0.59, the filling degree of the primary is 91%, and the contribution of the third light are 19.0($\pm$0.76)%, 20.4($\pm$0.72)%, 23.5($\pm$0.69)% and 24.6($\pm$0.68)% for B, V, R_c and I_c bands. On the right of Figure 6 are the theoretical light curves and the semi-detached configuration at the phase of 0.25.

5 DISCUSSION AND CONCLUSIONS

5.1 Orbital Period Evolution

Previous $O-C$ analysis could not describe the changes of the last decade, 2009–2019 (Qian 2002; Samec et al. 2006; Kim et al. 2009). Therefore, we collected all of the available data along with our observations and proposed a new model to re-analyse the $O-C$ curve of XZ CMi. It is found that our new $O-C$ model could well depict the orbital period changes of XZ CMi.

(*i*). Long-term period change.

The $O-C$ data spanning for over 100 yr where the rate of period change is $8.15(\pm2.14)\times10^{-9}$ d yr^{-1}. Since the mass of the primary component is estimated as 1.52($\pm$0.04) $M_\odot$, and the mass ratio in Figure 5 is 0.59, the mass of the secondary star of the eclipsing binary XZ CMi is detected to be 0.89($\pm$0.03) $M_\odot$. Thus, the mass transfer rate under conservative process can be derived from this equation,

$$\frac{\dot{P}}{\dot{m}_2}=3P(\frac{1}{m_2}-\frac{1}{m_1}). \quad (2)$$

It is calculated to be about $\dot{m}_2 = 1.0(\pm0.3)\times10^{-8}\ M_\odot$ yr^{-1}, which is exactly at the thermal time scale. This is in accord with the semi-detached configuration, where the low massive secondary star has filled the Roche lobe and continuously transferring matter to the more massive primary. However, it should be noted that the gas stream might temporarily break up along with the elongation the semi major axis, which means that the above mass transfer ratio may be varying (Zhang et al. 2014). According to Tout & Eggleton (1988) and Tout & Hall (1991), close binary with high filling degree should undergo an enhanced stellar wind and cause a large quantity of mass and angular momentum loss. However, Figure 5 shows that the orbital period of XZ CMi is increasing, which suggests that the influence of mass transfer is greater than that of mass and angular momentum loss.

(*ii*). Orbital period modulation.

The cyclic variation in the $O-C$ diagram is due to the light travel time effect caused by an eccentric companion star going around the central binary. Such model was first proposed by Irwin (1952) then successfully and widely applied to numerous variables and binary systems (Qian 2001; Qian et al. 2008; Zhu et al. 2012; Li & Qian 2014; Zhu et al. 2019a; Wang et al. 2019; Zhu et al. 2019b). Minimum mass of the third body is 0.42($\pm$0.09) $M_\odot$, while its maximum semi major axis is 25.2($\pm$5.7) au. It could be estimated that the light contribution of the third star is around 1% (Eddington 1924). The third star goes around the central binary pair by a 0.86($\pm$0.04) eccentric orbit once every 95.7($\pm$2.1) yr.

As for cyclic variation in the $O-C$ curve, Applegate mechanism has also been applied to some late type systems (Applegate 1992). Therefore, we should check and discuss whether it is efficient in XZ CMi.

$$\frac{\Delta P}{P}=-9\frac{\Delta Q}{ma^2}, \quad (3)$$

where a is the separation between the two stars in the eclipsing binary. Since Rovithis-Livaniou et al. (2000) had provided a formula to acquire the ΔP, i.e., $\Delta P = A\sqrt{2[1-\cos(2\pi P/P_3)]}$. As a result $\Delta P/P = 4.80156\times10^{-6}$. The simplified Kepler's third law is written as $(m_1+m_2)P^2 = 0.0134a^3$, where a is able to figure out. Consequently, the calculated $\Delta Q = 7.0\times10^{49}$ g cm^2, which is not within the range of $10^{50}-10^{52}$ g cm^2 for Algol binaries (Lanza & Rodonò 1999), revealing that the Applegate mechanism may not be a cause for the cyclic modulation of XZ CMi.

5.2 Visual System

We took an image of the ViS by the VR_CI_C bands at a 'good-seeing' night with the 2.16 m telescope on 2019 May 1 (Fig. 2). It is found that this dim 'Visual Star' gradually brightened along with the wavebands. We use IRAF aperture photometry to measure the brightness of the two visual stars, of which the light contribution in the VR_cI_c bands are separately 18.8%, 21.2% and 22.2%.

By checking the *Gaia* DR2 database (Gaia Collaboration et al. 2018), a target of 11.89 mean apparent magnitude in the *Gaia*-g band is located at an angular distance of 2.408 arcsec east by south of the eclipsing binary XZ CMi. Table 5 shows the parallaxes of XZ CMi (i.e., 3.1843$\pm$0.0423 mas) and the ViS (i.e., 3.2457$\pm$0.0532 mas) from the *Gaia* DR2 database. They are scarcely less within the range of errors. Moreover, the proper motion in two directions for XZ CMi are –16.64($\pm$0.077) and –8.577($\pm$0.053) mas yr^{-1}, and as for the ViS are –15.459($\pm$0.095) and –8.582($\pm$0.098) mas yr^{-1}

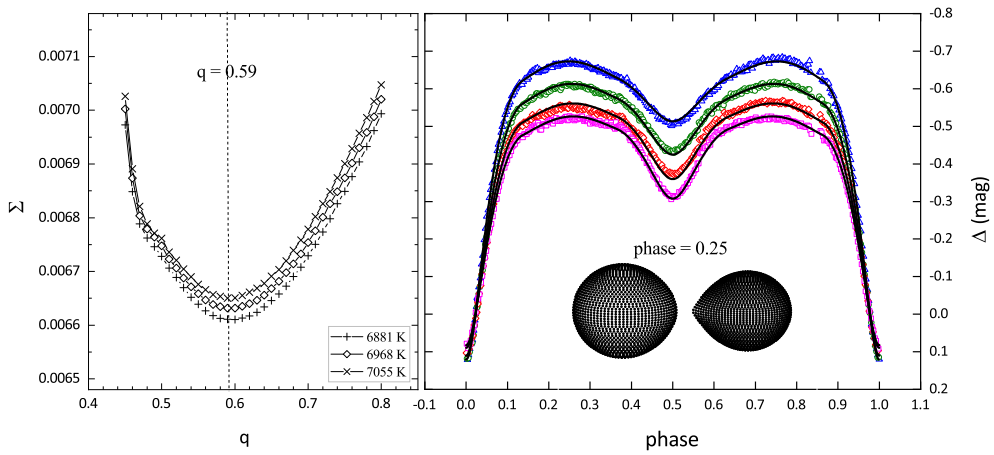

Fig. 6 *Left*: The $q - \Sigma$ relation with the lowest $q = 0.59$. *Right*: Theoretical light curves of XZ CMi and the configuration at the phase of 0.25.

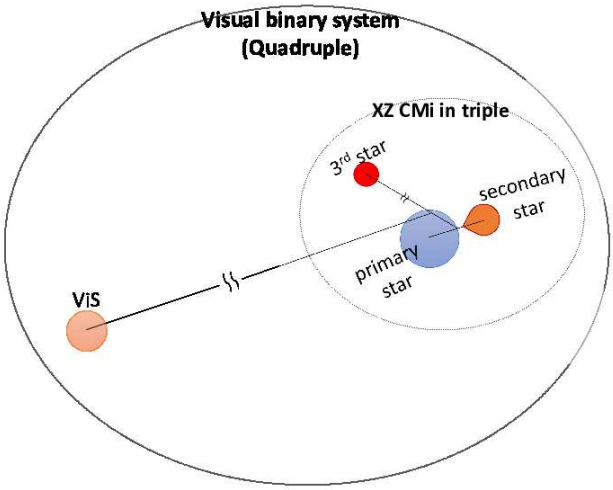

Fig. 7 A schematic diagram of this quadruple system.

(Gaia Collaboration et al. 2018). Noticing that the proper motion in right ascension direction is close but with the difference of about 1 mas yr^{-1}. Almost all of the astrometric parameters of the two visual points (i.e., α, δ, parallax and the proper motion of the declination component) reveal that it is most likely a visual and gravitational bound system. The dim ViS is located at a distance of about 760 au away from XZ CMi on the horizon plane of the celestial sphere; thus, the corresponding period is estimated to be about 10 480 yr.

By referring to the LAMOST DR6 catalogue, the head file of XZ CMi records that the input coordinate of this observation is originally intended for XZ CMi (i.e., $118.529448°$, $3.6556346°$), whereas actually pointed to the ViS (i.e., $118.530084°$, $3.655476°$). Unintentionally, the values of the atmospheric parameters of the visual companion are obtained by the 'mistake' of LAMOST on 2014 Nov 9. According to the LAMOST DR6 database, the effective temperature of the ViS is 6164($\pm$18) K, the gravitational constant $\log g = 4.61(\pm 0.03)$ cm s^{-2} and the metal abundance [Fe/H] equals 0.108($\pm$0.014) dex. It can be estimated that the mass of the ViS is 1.15 $M_\odot$ as a main sequence star. We performed the spectroscopic observations on 2019 May 1 and 2019 May 2 to have obtained the atmospheric parameters of XZ CMi. The surface temperature, $\log g$, and [Fe/H] of the ViS are all different from that of the parameters of the central triple observed in May 2019. Since the values of [Fe/H] of them are different (Table 2), it is difficult to believe that they were born from the same nebula. We might infer that the ViS was somehow captured from the interstellar field. It should be noted that the value of [Fe/H] for the ViS is actually higher than that of the in-

Table 4 Photometric Solutions of XZ CMi

Parameter	Value	Value	Value
mode	mode 5	mode 5	mode 5
T_1 (K)	6881	6968	7055
T_1/T_2	0.7054(±0.0011)	0.7031(±0.0011)	0.7006(±0.0011)
$q = M_2/M_1$	0.6122(±0.0090)	0.5900(±0.0089)	0.5900(±0.0092)
$i(^\circ)$	81.38 (±0.23)	81.50 (±0.31)	81.53 (±0.29)
f_1 [%]	91.37 (±0.34)	91.43 (±0.34)	91.49 (±0.35)
$r_{1\mathrm{pole}}/a$	0.3674(±0.0012)	0.3705(±0.0012)	0.3705(±0.0012)
$r_{2\mathrm{pole}}/a$	0.3163(±0.0012)	0.3132(±0.0012)	0.3131(±0.0012)
$r_{1\mathrm{point}}/a$	0.4274(±0.0018)	0.4307(±0.0019)	0.4308(±0.0017)
$r_{2\mathrm{point}}/a$	0.4502(±0.0012)	0.4463(±0.0012)	0.4463(±0.0012)
$r_{1\mathrm{side}}/a$	0.3838(±0.0014)	0.3871(±0.0014)	0.3872(±0.0014)
$r_{2\mathrm{side}}/a$	0.3306(±0.0013)	0.3273(±0.0013)	0.3272(±0.0013)
$r_{1\mathrm{back}}/a$	0.4030(±0.0015)	0.4063(±0.0015)	0.4063(±0.0014)
$r_{2\mathrm{back}}/a$	0.3628(±0.0012)	0.3595(±0.0013)	0.3594(±0.0013)
$l_{1B}/(l_{1B}+l_{2B})$	0.9237(±0.0007)	0.9260(±0.0008)	0.9260(±0.0008)
$l_{1V}/(l_{1V}+l_{2V})$	0.8772(±0.0011)	0.8805(±0.0013)	0.8804(±0.0012)
$l_{1Rc}/(l_{1Rc}+l_{2Rc})$	0.8437(±0.0014)	0.8481(±0.0016)	0.8481(±0.0016)
$l_{1Ic}/(l_{1Ic}+l_{2Ic})$	0.8128(±0.0017)	0.8176(±0.0019)	0.8174(±0.0019)
$l_{3B}/l_{\mathrm{total}B}$	0.1996(±0.0060)	0.1902(±0.0076)	0.1901(±0.0075)
$l_{3V}/l_{\mathrm{total}V}$	0.2121(±0.0057)	0.2039(±0.0072)	0.2038(±0.0070)
$l_{3Rc}/l_{\mathrm{total}Rc}$	0.2423(±0.0056)	0.2352(±0.0069)	0.2351(±0.0067)
$l_{3Ic}/l_{\mathrm{total}Ic}$	0.2517(±0.0057)	0.2455(±0.0068)	0.2454(±0.0067)
$\Sigma\,\mathrm{res}^2$	0.00004369	0.00004395	0.00004422

Table 5 Astrometric Parameters of XZ CMi and the ViS

Target	α_{2000} (deg)	δ_{2000} (deg)	Parallax (mas)	pm.ra (mas yr^{-1})	pm.dec (mas yr^{-1})
XZ CMi	118.529449945	3.65565080181	3.1843 (±0.0423)	–16.647 (±0.077)	–8.577 (±0.053)
the ViS	118.530102928	3.65551225130	3.2457 (±0.0532)	–15.459 (±0.095)	–8.582 (±0.098)

teracting binary. Thus, we can find that the ViS is a younger joint member of this wide binary system.

5.3 Photometric Solutions and Third Light Paradox

There were great differences of opinion about the temperature of the primary star of XZ CMi in history (Rafert 1990; Terrell & Wilson 1990; Terrell & Henden 2002; Kim et al. 2009). In this case, the q that they obtained ranges from 0.293 to 0.830, without consistent result. Moreover, the third light derived by many previous researchers from photometric solution is quite large, to be about 20%. Meanwhile, the mass of the third-star calculated though their $O-C$ method is rather low, which could contribute only 1% of the light. So the contradiction and paradox between the third-light and the third-body is remain unsolved for years.

By modelling the light curves, we found that the eclipsing binary XZ CMi is a semidetached system. Three temperatures show almost the same results, e.g., $q = 0.59$, $i = 81.5^\circ$, $f_1 = 91\%$, suggesting that the results are reliable and it is a near contact semidetached binary. According to the photometric solutions in Table 4, the third light are 19.0(±0.76)%, 20.4(±0.72)%, 23.5(±0.69)% and 24.6(±0.68)% for the B, V, R_C and I_C bands.

As we can see from this discussion (subsection of Orbital Period Evolution and subsection of Visual System), by summing the light contribution of the third star (the $O-C$ third star) and the light contribution of the fourth star (the ViS), it is just in accord with the results of the third-light proportion in the photometric solutions. As a result, this issue has been solved.

We demonstrate that the XZ CMi system is actually a hierarchical quadruple system. It consists of a close-in triple and a wide visual companion star shown in Figure 7. The eclipsing binary XZ CMi is located in the innermost layer of that close-in triple system. The ViS is possibly a gravitational bound fourth star located at the outer layer of this hierarchical quadruple system.

Acknowledgements This work is partly supported by the National Natural Science Foundation of China (Grant No. 11922306), the Key Science Foundation of Yunnan Province (Grant No. 2017FA001) and the CAS Interdisciplinary Innovation Team. The data were observed by using the Xinglong Tsinghua-NAOC 80 cm telescope, the NAOC 2.16 m telescope, and the Yunnan Observatories' 60 cm and 1 m telescopes. Additionally, the Guo Shou Jing Telescope (the Large Sky Area Multi-Object Fiber Spectroscopic Telescope LAMOST) is a National Major Scientific Project built by the Chinese Academy of Sciences. Funding for the project

has been provided by the National Development and Reform Commission. LAMOST is operated and managed by the National Astronomical Observatories, Chinese Academy of Sciences. This work has also made use of data from the European Space Agency (ESA) mission *Gaia* (https://www.cosmos.esa.int/gaia), processed by the *Gaia* Data Processing and Analysis Consortium (DPAC, https://www.cosmos.esa.int/web/gaia/dpac/consortium). Funding for the DPAC has been provided by national institutions, in particular the institutions participating in the *Gaia* Multilateral Agreement.

References

Applegate, J. H. 1992, ApJ, 385, 621
Cui, X. 2009, American Astronomical Society Meeting Abstracts, 213, 226.01
Dueball, J., & Lehmann, P. B. 1965, Astronomische Nachrichten, 288, 167
Eddington, A. S. 1924, MNRAS, 84, 308
Gaia Collaboration, Brown, A. G. A., Vallenari, A., et al. 2018, A&A, 616, A1
Gimenez, A., & Costa, V. 1979, Information Bulletin on Variable Stars, 1643
Hamers, A. S., & Samsing, J. 2019, arXiv:1904.09624
Hoffmeister, C. 1934, Astronomische Nachrichten, 253, 195
Huang, F., Li, J.-Z., Wang, X.-F., et al. 2012, RAA (Research in Astronomy and Astrophysics), 12, 1585
Hubscher, J. 2015, Information Bulletin on Variable Stars, 6152
Irwin, J. B. 1952, ApJ, 116, 211
Jiménez-Esteban, F. M., Solano, E., & Rodrigo, C. 2019, AJ, 157, 78
Kim, C.-H., Park, J.-H., Lee, J. W., & Jeong, J.-H. 2009, Journal of Astronomy and Space Sciences, 26, 140
Kouwenhoven, M. B. N., Goodwin, S. P., Parker, R. J., et al. 2010, MNRAS, 404, 1835
Lanza, A. F., & Rodonò, M. 1999, A&A, 349, 887
Lause, F. 1938, Astronomische Nachrichten, 266, 237
Li, L. J., & Qian, S. B. 2014, MNRAS, 444, 600
Lucy, L. B. 1967, ZAp, 65, 89
Mardirossian, F., & Giuricin, G. 1981, A&A, 96, 415
Motte, F., Andre, P., & Neri, R. 1998, A&A, 336, 150
Qian, S. 2001, AJ, 122, 2686
Qian, S. 2002, MNRAS, 336, 1247
Qian, S.-B., He, J.-J., Zhang, J., et al. 2017, RAA (Research in Astronomy and Astrophysics), 17, 087
Qian, S.-B., Li, L.-J., He, J.-J., et al. 2019a, RAA (Research in Astronomy and Astrophysics), 19, 001
Qian, S.-B., Liao, W.-P., & Fernández Lajús, E. 2008, ApJ, 687, 466
Qian, S.-B., Shi, X.-D., Zhu, L.-Y., et al. 2019b, RAA (Research in Astronomy and Astrophysics), 19, 064
Qian, S. B., Zhang, J., He, J. J., et al. 2018, ApJS, 235, 5
Rafert, J. B. 1990, AJ, 100, 1253
Rovithis-Livaniou, H., Kranidiotis, A. N., Rovithis, P., & Athanassiades, G. 2000, A&A, 354, 904
Ruciński, S. M. 1969, Acta Astronomica, 19, 245
Samec, R., Rook, I. B., Faulkner, D. R., Hawkins, N. C., & van Hamme, W. 2006, The Observatory, 126, 255
Samolyk, G. 2009, Journal of the American Association of Variable Star Observers (JAAVSO), 37, 44
Terrell, D., Gunn, J. B., & Kaiser, D. H. 1994, PASP, 106, 149
Terrell, D., & Henden, A. A. 2002, Information Bulletin on Variable Stars, 5310
Terrell, D., & Wilson, R. E. 1990, PASP, 102, 646
Tout, C. A., & Eggleton, P. P. 1988, MNRAS, 231, 823
Tout, C. A., & Hall, D. S. 1991, MNRAS, 253, 9
van Hamme, W. 1993, AJ, 106, 2096
Wang, Z.-H., Zhu, L.-Y., Li, L.-J., & Tian, X.-M. 2019, RAA (Research in Astronomy and Astrophysics), 19, 107
Wilson, R. E. 1979, ApJ, 234, 1054
Wilson, R. E., & Devinney, E. J. 1971, ApJ, 166, 605
Zejda, M., Mikulasek, Z., & Wolf, M. 2006, Information Bulletin on Variable Stars, 5741
Zhang, J., Qian, S.-B., & Jiang, L.-Q. 2014, RAA (Research in Astronomy and Astrophysics), 14, 179
Zhang, J., Qian, S.-B., Wu, Y., & Zhou, X. 2019, ApJS, 244, 43
Zhao, G., Zhao, Y.-H., Chu, Y.-Q., Jing, Y.-P., & Deng, L.-C. 2012, RAA (Research in Astronomy and Astrophysics), 12, 723
Zhu, L., Qian, S.-B., & Li, L. 2012, PASJ, 64, 94
Zhu, L.-Y., Tian, X.-M., Zhou, X., Li, L.-J., & Wang, Z.-H. 2019a, RAA (Research in Astronomy and Astrophysics), 19, 094
Zhu, L. Y., Wang, Z. H., Tian, X. M., Li, L. J., & Gao, X. 2019b, MNRAS, 489, 2677